University of Bristol - Explore Bristol Research
General rights

Design and Characterisation of a Muscle-Mimetic Dielectrophoretic Ratcheting Actuator

Martin Garrad [ID], Mohammad Naghavi Zadeh, Christian Romero [ID], Fabrizio Scarpa,
Andrew T. Conn [ID], *Member, IEEE*, and Jonathan Rossiter

Abstract—The high potential impact of soft robotics is hampered by a lack of actuators that combine high-force, high-work and high-power capabilities, limiting application in real-world problems. Typically, soft actuators are tuned to an application by gearing - for example, trading power for strain. An example of a recently developed soft-actuator which exploits such gearing is the dielectrophoretic liquid zipping (DLZ) actuator. DLZs can produce large strains ($> 99\%$) and power densities comparable to biological muscles, but cannot achieve both in a single actuator. In this work, we introduce a muscle-mimetic DLZ ratcheting actuator (DLZ-R) that allows multiple DLZ-R heads to operate in parallel, thereby increasing force output without sacrificing stroke or power. We first characterise the effect of geometry on the performance of a 1-head DLZ-R, before demonstrating that the force, work, and power output of the DLZ-R scale linearly with the number of active DLZ heads. Next, we investigate the relationship between driving frequency and power output. Finally, we demonstrate a 12-head DLZ ratchet. We believe the DLZ-R represents a step towards soft actuators that can provide both high-work and high-power and the widespread use of soft technologies.

Index Terms—Soft sensors and actuators, soft robot materials and design.

Martin Garrad, Mohammad Naghavi Zadeh, Christian Romero, and Jonathan Rossiter are with the Department of Engineering Mathematics, University of Bristol, Bristol BS8 1TW, U.K., and also with the SoftLab, Bristol Robotics Laboratory, University of Bristol and University of the West of England, Bristol , U.K. (e-mail: m.garrad@bristol.ac.uk; m.naghavizadeh@bristol.ac.uk; cr16031@bristol.ac.uk; jonathan.rossiter@bris.ac.uk).

Fabrizio Scarpa is with the Department of Mechanical Engineering, University of Bristol, Bristol BS8 1TR, U.K., and also with the Bristol Composites Institute, University of Bristol, Bristol , U.K. (e-mail: f.scarpa@bristol.ac.uk).

Andrew T. Conn is with the Department of Mechanical Engineering, University of Bristol, Bristol BS8 1TR, U.K., and also with the SoftLab, Bristol Robotics Laboratory, University of Bristol and University of the West of England, Bristol , U.K. (e-mail: a.conn@bristol.ac.uk).

This letter has supplementary downloadable material available at https://doi.org/10.1109/LRA.2022.3149039, provided by the authors.

Digital Object Identifier 10.1109/LRA.2022.3149039
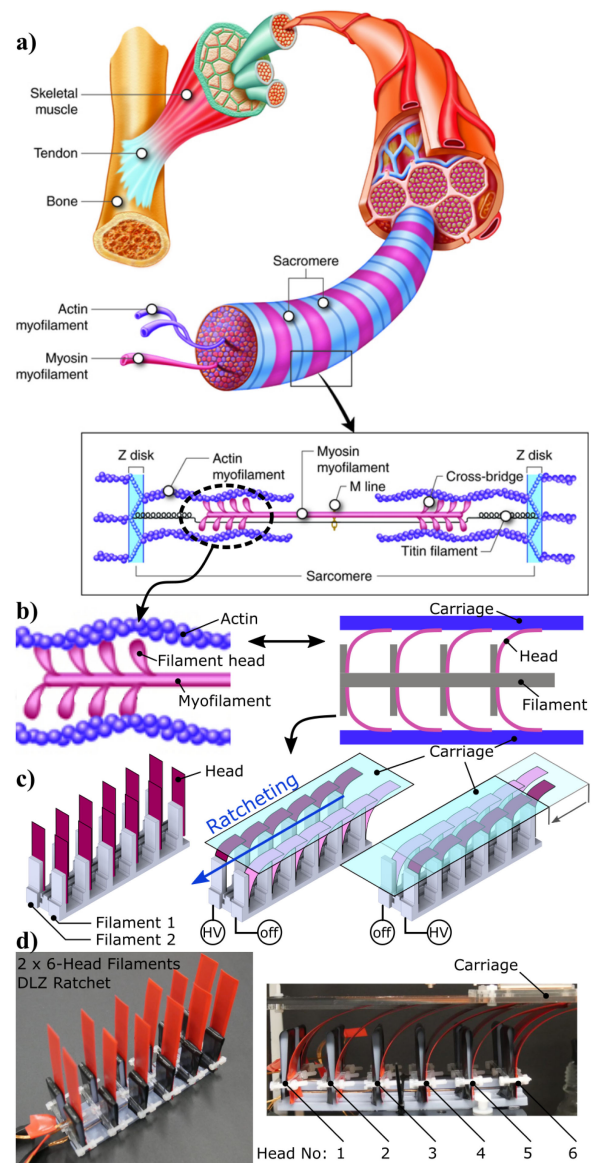
Fig. 1. The Dielectrophoretic Liquid Zipping Ratchet (DLZ-R). (a) The DLZ-R is inspired by the architecture of biological muscle sarcomeres, in which myosin filaments generate work by sequentially acting on an actin fibre. (CC BY-NC-SA). (b) Myosin generates work by undergoing a sequence of *attachment*, *power-stroke*, *detachment* and *return-stroke*. In the DLZ-R, we use electro-adhesion to mimic the process of attachment-detachment, dielectrophoretic liquid zipping to mimic the power-stroke and elastic energy storage to mimic the return-stroke. (c) Rendering of a DLZ-R. A DLZ-R consists of two parallel DLZ filaments, with each filament driven in antiphase. (d) Images of a 2-filament, 12 head DLZ-R.

I. INTRODUCTION

THE development of soft machines and robots could enable a new generation of autonomous systems that can operate in unpredictable and unstructured environments [1]–[3]. In turn, this could enable new applications in bio-medicine [4], ecology [5] and virtual reality [6]. However, this vision is currently held back by the limited performance of soft actuators. In particular, soft actuators cannot produce high-force, high-work and high-power in a single configuration.

Instead, existing soft actuators typically fall into two classes: high-work or high power. High-work density actuators, such as shape-memory alloys (SMA) or fluidic elastomer actuators (FEA) can generate large forces relative to their weight. Recent developments in this area include an ethanol-silicone foam [7], a plant inspired osmotic actuator [8], pouch motors driven by the evaporation of low-boiling point fluids [9], [10] and thermally driven coiled polymer actuators [11]. However, despite impressive force and work outputs, these actuators suffer from a slow relaxation time, limiting their power output and range of suitable applications.

In contrast, high-power soft actuators, such as dielectric elastomer actuators (DEAs) and ionic-polymer metal composites (IPMCs) are capable of operating at high-frequency, but struggle to produce large forces or strains [12]–[14]. This trade-off between high work and high power severely limits the applications of soft robotic technologies.

Recently, electrostatic actuators have received renewed interest within soft robotics [15]–[17]. One example of such an actuation technology is dielectrophoretic liquid zipping (DLZ) [18]. A DLZ actuator consists of two flexible electrodes separated by a thin insulating layer. When a high voltage is applied between the two electrodes, electrostatic forces cause the electrodes to be attracted to each other, generating large strains as the two electrodes *zip* together. A small drop of dielectric liquid placed in the hinge between the two electrodes and held in place by dielectrophoretic forces, amplifies the electrostatic forces up to 40x. High-force, high-work and high-power DLZ configurations have been demonstrated. However, these capabilities cannot be combined in a single actuator. For example, to achieve high-force operation in [18], a configuration with small stroke must be used, which limits both work and power output.

One approach to achieving both high-force and high-power soft actuators is to use a mechanism which increases force without requiring a reduction in strain or frequency. In biological muscle, this is achieved by a ratcheting configuration (Fig. 1(a) & (b)) [19], [20]. Within each sarcomere, work is generated by the cyclic activation of myosin heads acting on actin fibres (Fig. 1(b)). First, myosin *attaches* to the actin fibre. Next, the myosin undergoes a *power-stroke*, driving the actin fibre forwards. The myosin head then *detaches* from the actin fibre and undergoes a *return-stroke*, restoring it to its initial configuration and enabling the cycle to begin again.

Taking inspiration from this approach, we introduce the dielectrophoretic liquid zipping ratchet (DLZ-R). A DLZ-R consists of two *filaments*, with each filament containing one or more *heads*. The DLZ-R uses electro-adhesion [21] to mimic the attachment and detachment of the myosin head,

dielectrophoretic liquid zipping to mimic the power-stroke and elastic energy release to mimic the return stroke.

The main contributions of this paper are:
- Introduction of the DLZ-R concept.
- Investigation of the effect of geometry, operating frequency and number of active heads on the performance of the DLZ-R.
- Demonstration of a 2-filament, 12-head DLZ-R.

We proceed by first reviewing the physical principles of the DLZ-R. We then perform a parametric investigation of a 1-head DLZ filament, elucidating the relationship between geometry and performance. Next, we show the operation of a multi-head DLZ filament, demonstrating that force, work and power output scale with the number of active heads. Finally, we investigate the relationship between frequency and power, before demonstrating a 2-filament, 12-head DLZ-R that achieves an average power of 0.1 mW. Although less than the power generated by human muscle or best-in-class artificial muscles [22], we believe the ability to increase force, work and power output simultaneously marks the DLZ-R as a route towards soft robotic actuators with both high-force and high-power and a further step towards autonomous and capable soft robots.

II. PRINCIPLE OF OPERATION

A DLZ-R consists of two filaments driven in antiphase, with each filament containing one or more DLZ-R heads. Each head consists of a slender spring steel beam (length = 180 mm, thickness = 0.1 mm, width = 12 mm, Prazisionsfolien, Germany) covered with two layers of PVC tape. The beams are clamped to a rigid acrylic *zipping wall*, covered first with copper tape and then a further layer of PVC tape. Each beam is pre-compressed into a bent configuration by contact with the ratchet output carriage. This carriage consists of an acrylic plate attached to a linear slider (BSP1045SL IKO Nippon Thompson, Japan), also covered on the lower side with a layer of copper tape and a layer of PVC tape.

Fig. 2 shows the structure of a DLZ-R head and defines the key geometric parameters. In particular, we introduce the shape parameter $L^* = L_{\text{compress}}/L$, which denotes the ratio of the distance between the bottom of the DLZ-R head and the output carriage, L_{compress}, to the spring steel beam length, L. L^* determines the initial configuration of a DLZ-R head, with smaller L^* corresponding to beams with a greater amount of bending. This affects the performance of the DLZ-R head by decreasing the zipping angle, θ_{zip}, and increasing the electro-adhesion length, L_{adhesion}. Intuitively, this can be thought of as biasing the head towards greater zipping forces at the expense of lower electro-adhesive forces. The effect of other parameters, such as beam length, thickness and Young's modulus on dielectric zipping forces have previously been explored [18] and are considered outside the scope of this work.

Upon application of high-voltages to the DLZ-R head, two phenomena occur simultaneously to generate work. At the interface between the head and the carriage, electrostatic forces lead to electro-adhesion, mimicking the attachment of the myosin head. At the same time, electrostatic forces attract the head to the zipping wall, causing it to zip. These forces cause the
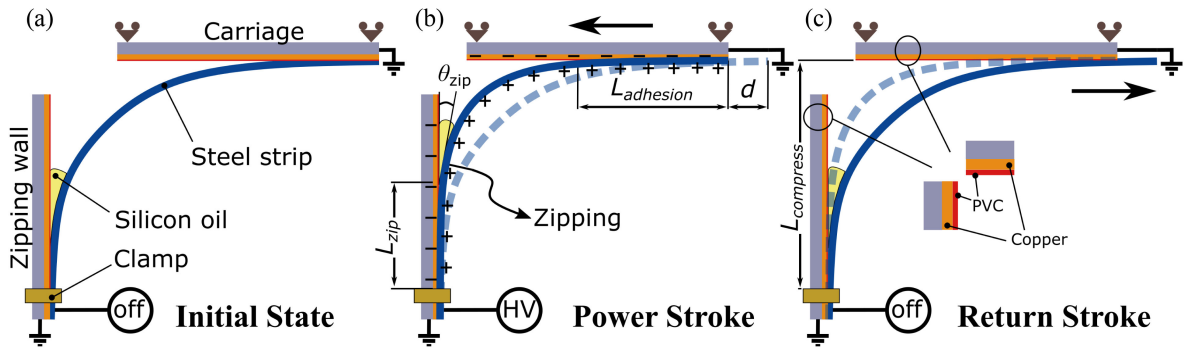
Fig. 2. DLZ-R principle of operation. (a) A DLZ-R filament consists of a spring steel beam covered with two layers of PVC tape, an acrylic zipping wall, and an acrylic carriage both covered with a layer of copper tape and insulated with a single layer of PVC tape. (b) When high-voltage is placed on the beam, electro-adhesive forces act between the beam and the carriage. Simultaneously, zipping forces cause the beam to deform elastically. The restoring forces in the beam are resisted by the zipping wall and transmitted to the carriage, leading to forward movement of the carriage. (c) When high-voltage is removed, both electro-adhesive and zipping forces also disappear. This allows release of the elastic energy stored in the beam, which returns to its original configuration. Without electro-adhesive forces acting between the carriage and the beam, the beam slides over the carriage, leading to a net displacement in the forward direction.
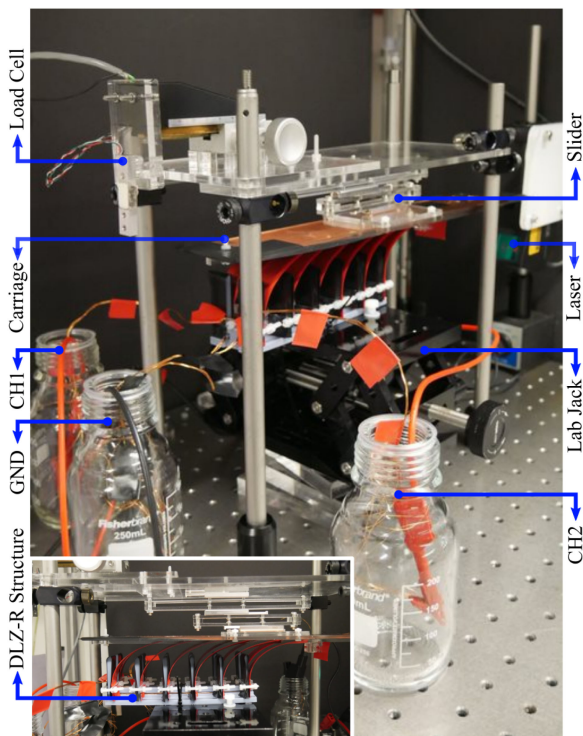

Fig. 3. Experimental setup. The DLZ-R carriage is attached to a linear slider, with the DLZ-R heads mounted on a lab-jack. A load cell is used to measure blocking force, while a laser displacement meter is used to measure displacement in isotonic tests. The DLZ-R is attached to a fixed mass via a pulley (not shown) for isotonic testing.

Fig. 4. Effect of geometry on blocking force. (a) Plots the blocking force due to zipping alone, when the DLZ-R head is clamped to the carriage, while (b) Plots the blocking force when the zipping force is transmitted by electro-adhesion. In both plots, results are the mean of three trials and error bars represent one standard error.

beam to deform until the electrostatic forces are balanced by the elastic restoring force. Further details about the dielectric zipping forces can be found in [18], while further information about electro-adhesion can be found in [23].

When the high-voltage is removed from the beam, both the electrostatic and zipping forces disappear. The elastic energy in the beam is then released, causing the beam to return to its original configuration. Without electro-adhesion attracting the beam to the carriage, the beam slides over the surface of the carriage during its return stroke, leading to a net movement

over the cycle and mimicking the return stroke of the myosin head. Note that the power and return strokes place competing requirements on the bending stiffness of a DLZ head, with the power-stroke requiring low bending stiffness to maximise displacement, while the return-stroke requires high bending stiffness for fast and reliable operation.

Fig. 5. Isotonic characterisation of a single DLZ-R head. Top panels show work output for loads of 2, 5 and 10 grams as L^* is varied from 0.3 to 0.8. Bottom panels show average power output for the same parameters. In all plots, results are the mean of three trials and error bars represent one standard error.

Fig. 6. Force throughout stroke for a single DLZ head. Results are the mean of three trials and error bars represent one standard error.

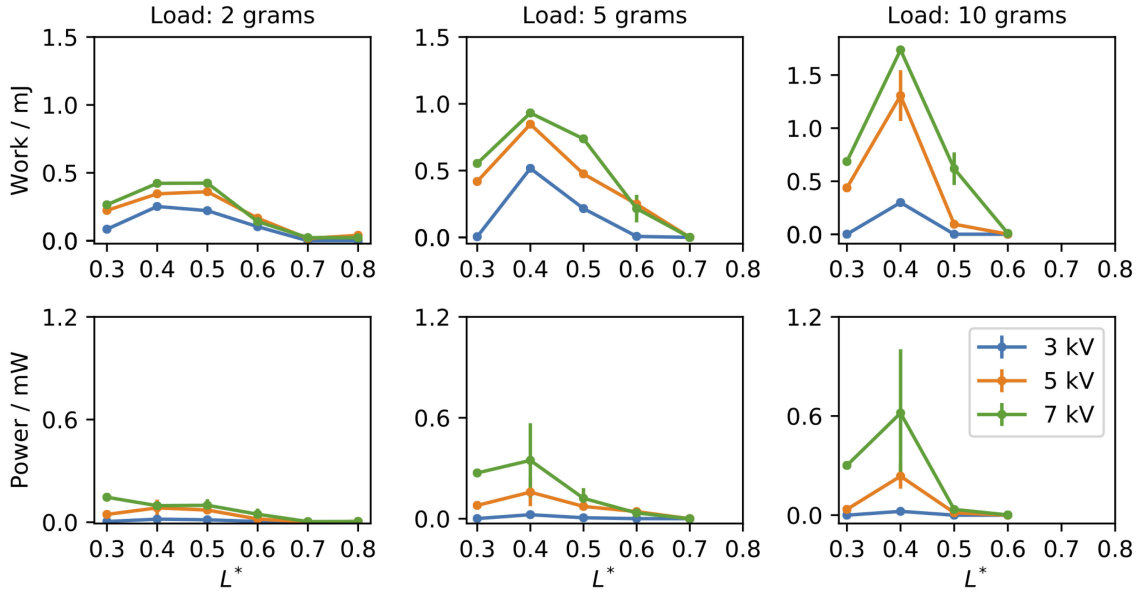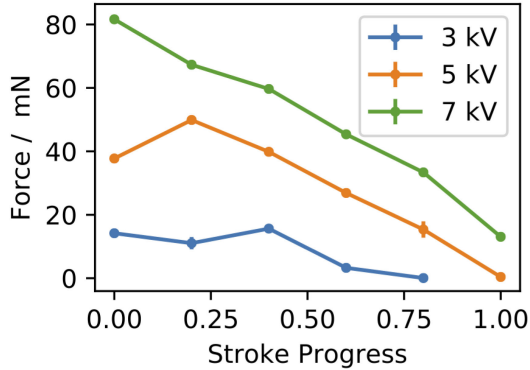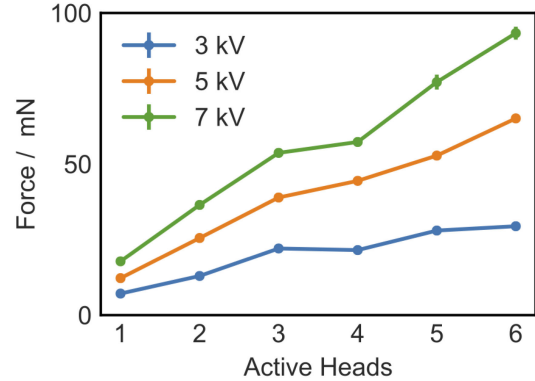Fig. 7. DLZ-R blocking force as the number of active heads is varied. Results are the mean of three trials and error bars represent one standard error.

We found that there were three mechanisms that may prevent a DLZ-R head from generating work. First, if θ_{zip} is too large, the electrostatic forces in the initial configuration are not strong enough to deform the beam. Secondly, a small $L_{adhesion}$ may limit the electro-adhesive forces between the DLZ-R head and the carriage, allowing the head to slip during the power stroke, and preventing transmission of force to the carriage. As decreasing θ_{zip} also leads to a decrease in $L_{adhesion}$, we performed a parametric investigation to understand the effect of L^* on the performance of a DLZ-R head and to allow us to identify the geometry that best balances zipping and electro-adhesive forces.

The work output of a DLZ-R head may also be reduced because of stiction between the carriage surface and head, likely due to the capillary forces acting between the two surfaces and the dielectric liquid as well as the slow relaxation of electro-adhesive forces [23]. If there is too much stiction, the beam does not slide over the carriage surface on the return stroke, leading to an oscillating, rather than ratcheting output. To prevent this from occurring, we designed our ratchet to consist of two

independently controlled DLZ-R filaments. By driving the two filaments in antiphase, we ensure that one filament is undergoing its power stroke, while the other is undergoing its return stroke.

III. RESULTS

A. Single Cycle Performance Characterisation of a 1-Head DLZ-R Filament

To allow us to understand the effect of head geometry, we investigated the relationship between L^* and performance. First, we explored how L^* affected the performance of a DLZ-R head independent of electro-adhesion. To do this, we used an acrylic clip to clamp the DLZ-R head to the output carriage and disconnected the carriage from the power supply. We measured the blocking force by applying a voltage to the DLZ-R head, while the carriage was pushed against a load cell (3132 Micro Load Cell, RobotShop). Fig. 3 shows a labelled picture of the experimental setup. Fig. 4(a) plots the blocking force. As L^* is increased from 0.3 to 0.7, the force increases. This is due to the
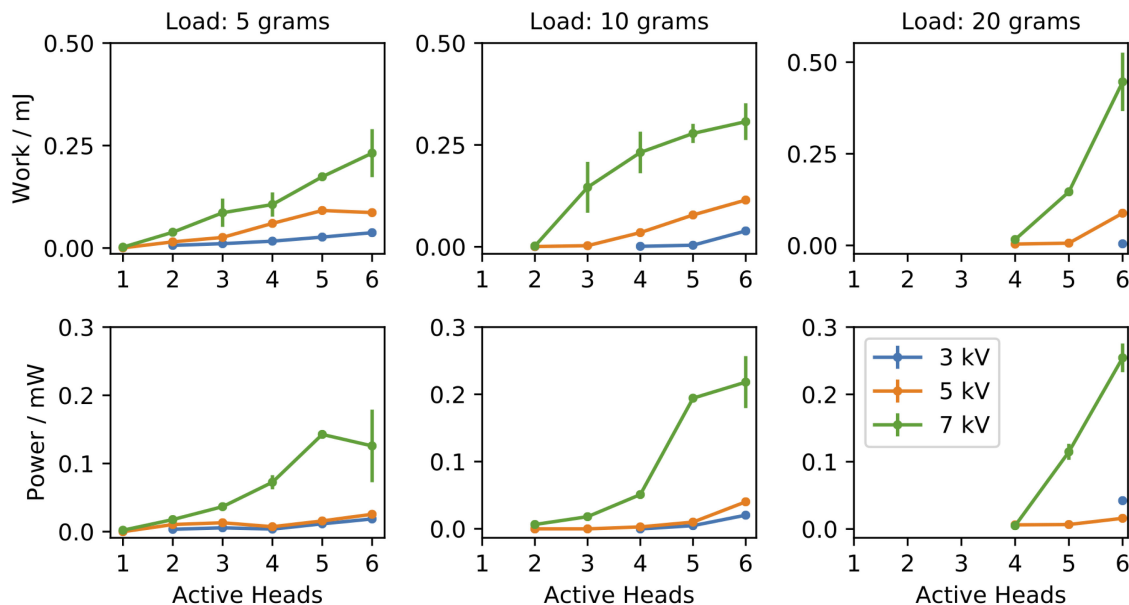
Fig. 8. Work and power amplification of a 6-head DLZ-R filament. Top panels show work output for loads of 5, 10 and 20 grams as the number of active heads is increased from 1 to 6. Bottom panels show average power for the same parameters. In all plots, results are the mean of three trials and error bars represent one standard error.

direction of the elastic restoring force becoming more aligned with the moving direction of the carriage as L^* increases. At $L^* = 0.8$, the force drops. This is because the beam deformation due to zipping reduces as L^* approaches 1.

To understand the effect of L^* on the electro-adhesion forces, we repeated these experiments without clamping the DLZ-R head and with the carriage re-connected to electrical ground. Fig. 4(b) plots the blocking force for the same range of L^* as above. Unlike the previous experiment, the force peaks at $L^* = 0.4$ for 7 kV. This suggests that at higher L^*, the reduction in $L_{adhesion}$ means the electro-adhesive forces are insufficient to transmit the zipping-induced bending forces. Note that the large error bars (for all Voltages) for $L^* = 0.5$ and 0.6 are due to the stochastic nature of the stick-slip interaction between the DLZ-R head and carriage. In some trials, the head is able to adhere to the carriage and transmit zipping forces. In other trials, the head slips before it has completed zipping, reducing the measured force. Note also that the forces are higher in the unclamped configuration for $L^* = 0.3$ and 0.4 as the clamp deforms the beam slightly away from the zipping wall, increasing θ_{zip} and reducing zipping forces.

To further understand the effect of L^*, we performed isotonic testing of a single DLZ head. To do this, we connected a mass to the carriage via a pulley, forcing the DLZ-R to lift the load against gravity and measured the displacement with a laser displacement meter (LKG-152, Keyence). Fig. 5 plots the work and average power output over a single cycle as L^* is varied for loads of 2, 5 and 10 grams. These tests confirmed that the greatest amount of work and power is generated at $L^* = 0.4$.

Finally, we measured the blocking force at a number of displacements (with the DLZ head clamped, and the carriage again disconnected) in order to understand how the force output of a DLZ-R head varies over a single cycle. Fig. 6 plots the measured force for voltages of 3, 5, and 7 kV. In general, the

force decreases linearly throughout the stroke. This suggests that a ratchet consisting of two DLZ-R filaments driven in antiphase will produce a saw-tooth output force.

B. Work and Power Scaling of a Multi-Head DLZ-R

Next, we show that by increasing the number of DLZ-R heads, we are able to increase the force, work and power output of a DLZ-R. To do this, we fabricated an actuator with 6 DLZ-R heads and varied the number of active heads. To realise the multi-head DLZ-R, we also reduced the length of each DLZ-R head (from L = 180 mm to L = 80 mm). As the stiffness of a slender beam is proportional to the cube of its length, we also reduced the thickness of each DLZ-R head (from t = 0.1 mm to 0.04 mm).

Fig. 7 plots the blocking force for the multi-head DLZ-R filament as we increase the number of active heads. The force increases linearly with the number of heads, suggesting that each head contributes additively to the total force output. Fig. 8 plots the work and average power output for the multi-head DLZ-R filament when evaluated isotonically with loads of 5, 10 and 20 grams. In both cases, performance increases with the number of active heads, confirming that the DLZ-R allows each quantity to be increased simultaneously. Note that the larger error bars for the 7 kV line are due to operating close to the breakdown voltage of the PVC tape, making the DLZ-R more sensitive to variation due to manufacturing.

C. Frequency and Power Output of a 2-Filament, 2-Head DLZ-R

Next, we investigated the relationship between driving frequency and power output for a 2-filament, 2-head DLZ-R (see Fig. 1(d)). For this test, we used a pair of DLZ filaments, driven with two out of phase 7 kV amplitude square waves. Fig. 9
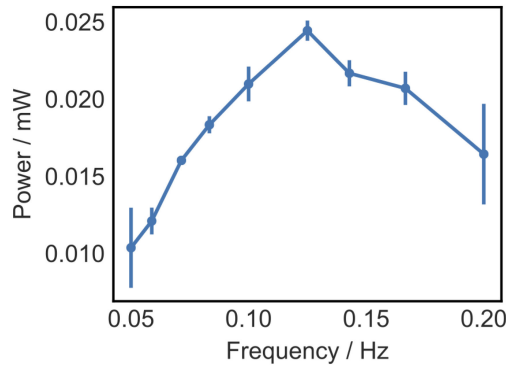
Fig. 9. Power and frequency. Power plotted against frequency for a 2-filament, 2-head DLZ-R working isotonically against a 2 g mass. Results are the mean of 3 trials and error bars represent one standard error.
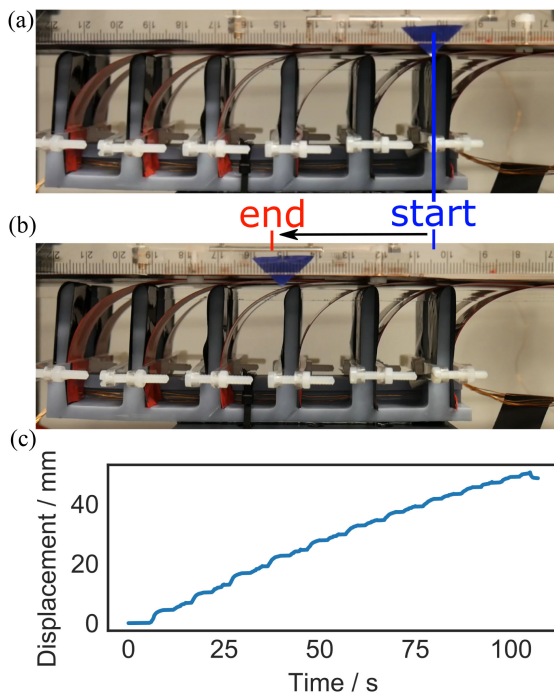

Fig. 10. Demonstration of a 2-filament, 12-head DLZ-R. (a) and (b) show displacement of the DLZ-R carriage as it lifts a 20 g mass against gravity. (c) shows the displacement of the carriage plotted against time.

IV. DEMONSTRATION OF A 2-FILAMENT, 12-HEAD DLZ-R

Finally, we demonstrate cyclic operation of a 2-filament, 12-head DLZ-R. Fig. 10 shows the displacement of the ratchet carriage when lifting a 20 g mass. The DLZ-R generates a total displacement of 50 mm in 100 seconds, corresponding to a speed of 0.5 mm/s and an average power of 0.1 mW.

V. DISCUSSION & CONCLUSIONS

In this paper, we have introduced the DLZ-R, a ratcheting actuator inspired by the sarcomeric structure of biological muscle. The DLZ-R uses electro-adhesion to mimic the attachment / detachment cycle of myosin heads and dielectrophoretic zipping and elastic energy storage to mimic the power and return strokes, respectively. We have introduced the shape parameter, L^*, which characterises the degree of bending in a resting head, and have shown that best performance is achieved with $L^* = 0.4$. We have further shown that our sarcomeric inspired structure allows the force, work and power output by the DLZ-R to be increased by increasing the number of DLZ-R heads. Finally, we have shown that the peak power output of a DLZ-R head is produced at a frequency of 0.125 Hz and demonstrated a 2-filament, 12-head DLZ-R with an average power output of 0.1 mW.

The 2-filament, 12-head DLZ-R has a total mass of 150 grams, corresponding to a specific power of 0.6 mW/kg. This is below the performance of typical human muscle (50 W/kg [22]) and also below the best performing artificial muscles such as those based on coiled polymers (27.1 W/kg [11]), multiwalled carbon nanotubes (27900 W/kg [25]), dielectric elastomer actuators (244 W/kg [26]) or pneumatic artificial muscles (10 W/kg [27]). However, in this proof-of-concept work, we optimised the design of the DLZ-R for simple manual fabrication and to enable facile addition or removal of DLZ-R heads. Single DLZ actuators have generated exceptionally high average power densities of 424 kW/m^3 [18], so future reductions in the mass and volume associated with each additional DLZ-R head can significantly increase the power density. Combined with the ability of the DLZ-R to increase force, work and power output by adding DLZ-R heads, this suggests a route towards high-power soft actuators.

Although the DLZ-R demonstrated in this work operates at the macro-scale, fabricating DLZ-Rs with large ($>$100) numbers of heads would require reducing the size of each head to instead operate on mm- or μ m length scales. As the flexural stiffness of a slender beam is proportional to the cube of its length, any reduction in length must be compensated for by changes in configuration which maintain the slenderness of the beam, and subsequent ability of the zipping forces to produce large deformations. One approach to maintain the slenderness of the beam would be to reduce the thickness, which also has a cubic relationship with the stiffness. However, limitations in fabrication techniques may limit the scale at which this approach can work.

Furthermore, although a large thickness reduces the power stroke displacement due to high strain energy, it also facilitates the return of the beam to the initial state in a shorter time, which helps to reduce the total cycle time. This suggests that as the size of the DLZ-R is reduced, it may also be necessary to adjust the value of L^*.

In this work, we have introduced the DLZ-R, a bio-inspired soft actuator based on electro-adhesion and dielectrophoretic liquid zipping. We have characterised the effect of geometry and control frequency on performance, and shown that the force,

plots the power generated when driving a load of 2 grams as the frequency is increased from 0.05 to 0.2 Hz. We measured the highest average power of 0.025 mW when operating at a frequency of 0.125 Hz.

The power output of the DLZ-R is limited by the time taken for the return stroke of each head. We believe this is predominantly due to the time taken for the polarisation of the dielectric liquid to relax back to its equilibrium configuration. This is a common problem in electro-adhesives [24] and causes adhesive forces to relax slowly, limiting the cycle frequency of the DLZ-R.

work and power of the DLZ-R can be increased by increasing the number of active heads. Finally, we have demonstrated a 2-filament, 12-head DLZ-R that can generate 0.1 mW. By enabling soft actuators to increase force, work and power in a single actuator, the DLZ-R represents a step towards widespread application of soft technologies.

REFERENCES

[1] C. Majidi, "Soft-matter engineering for soft robotics," *Adv. Mater. Technol.*, vol. 4, no. 2, 2019, Art. no. 1800477.

[2] D. Rus and M. T. Tolley, "Design, fabrication and control of soft robots," *Nature*, vol. 521, no. 7553, pp. 467–475, 2015.

[3] S. Kim, C. Laschi, and B. Trimmer, "Soft robotics: A bioinspired evolution in robotics," *Trends Biotechnol.*, vol. 31, no. 5, pp. 287–294, 2013.

[4] M. Cianchetti, C. Laschi, A. Menciassi, and P. Dario, "Biomedical applications of soft robotics," *Nature Rev. Mater.*, vol. 3, no. 6, pp. 143–153, 2018.

[5] S. Aracri *et al.*, "Soft robots for ocean exploration and offshore operations: A perspective," *Soft Robot.*, vol. 8, no. 6, pp. 625–639, 2021.

[6] J. Yin, R. Hinchet, H. Shea, and C. Majidi, "Wearable soft technologies for haptic sensing and feedback," *Adv. Funct. Mater.*, vol. 31, no. 39, 2020, Art. no. 2007428.

[7] A. Miriyev, K. Stack, and H. Lipson, "Soft material for soft actuators," *Nature Commun.*, vol. 8, no. 1, pp. 1–8, 2017.

[8] I. Must, E. Sinibaldi, and B. Mazzolai, "A variable-stiffness tendril-like soft robot based on reversible osmotic actuation," *Nature Commun.*, vol. 10, no. 1, pp. 1–8, 2019.

[9] R. Niiyama, X. Sun, C. Sung, B. An, D. Rus, and S. Kim, "Pouch motors: Printable soft actuators integrated with computational design," *Soft Robot.*, vol. 2, no. 2, pp. 59–70, 2015.

[10] M. Garrad, G. Soter, A. T. Conn, H. Hauser, and J. Rossiter, "Driving soft robots with low-boiling point fluids," in *Proc. 2nd IEEE Int. Conf. Soft Robot.*, 2019, pp. 74–79.

[11] C. S. Haines *et al.*, "Artificial muscles from fishing line and sewing thread," *Science*, vol. 343, no. 6173, pp. 868–872, 2014.

[12] U. Gupta, L. Qin, Y. Wang, H. Godaba, and J. Zhu, "Soft robots based on dielectric elastomer actuators: A review," *Smart Mater. Struct.*, vol. 28, no. 10, 2019, Art. no. 103002.

[13] C. Cao, X. Gao, S. Burgess, and A. T. Conn, "Power optimization of a conical dielectric elastomer actuator for resonant robotic systems," *Extreme Mechanics Lett.*, vol. 35, 2020, Art. no. 100619.

[14] S. Sareh, J. Rossiter, A. Conn, K. Drescher, and R. E. Goldstein, "Swimming like algae: Biomimetic soft artificial cilia," *J. Roy. Soc. Interface*, vol. 10, no. 78, 2013, Art. no. 20120666.

[15] E. Acome *et al.*, "Hydraulically amplified self-healing electrostatic actuators with muscle-like performance," *Science*, vol. 359, no. 6371, pp. 61–65, 2018.

[16] S. Schlatter, G. Grasso, S. Rosset, and H. Shea, "Inkjet printing of complex soft machines with densely integrated electrostatic actuators," *Adv. Intell. Syst.*, vol. 2, no. 11, 2020, Art. no. 2000136.

[17] R. Diteesawat, T. Helps, M. Taghavi, and J. Rossiter, "Electro-pneumatic pumps for soft robotics," *Sci. Robot.*, vol. 6, no. 51, 2021, Art. no. eabc3721.

[18] M. Taghavi, T. Helps, and J. Rossiter, "Electro-ribbon actuators and electro-origami robots," *Sci. Robot.*, vol. 3, no. 25, 2018, Art. no. eaau9795.

[19] J. M. Squire, "Architecture and function in the muscle sarcomere," *Curr. Opin. Struct. Biol.*, vol. 7, no. 2, pp. 247–257, 1997.

[20] R. K. Josephson, "Dissecting muscle power output," *J. Exp. Biol.*, vol. 202, no. 23, pp. 3369–3375, 1999.

[21] V. Cacucciolo, J. Shintake, and H. Shea, "Delicate yet strong: Characterizing the electro-adhesion lifting force with a soft gripper," in *Proc. 2nd IEEE Int. Conf. Soft Robot.*, 2019, pp. 108–113.

[22] S. M. Mirvakili and I. W. Hunter, "Artificial muscles: Mechanisms, applications, and challenges," *Adv. Mater.*, vol. 30, no. 6, 2018, Art. no. 1704407.

[23] J. Guo, J. Leng, and J. Rossiter, "Electroadhesion technologies for robotics: A comprehensive review," *IEEE Trans. Robot.*, vol. 36, no. 2, pp. 313–327, Apr. 2020.

[24] C. Cao, X. Gao, J. Guo, and A. Conn, "De-electroadhesion of flexible and lightweight materials: An experimental study," *Appl. Sci.*, vol. 9, no. 14, 2019, Art. no. 2796.

[25] M. D. Lima *et al.*, "Electrically, chemically, and photonically powered torsional and tensile actuation of hybrid carbon nanotube yarn muscles," *Science*, vol. 338, no. 6109, pp. 928–932, 2012.

[26] J. Li *et al.*, "Superfast-response and ultrahigh-power-density electromechanical actuators based on hierarchal carbon nanotube electrodes and chitosan," *ACS Nano Lett.*, vol. 11, no. 11, pp. 4636–4641, 2011.

[27] F. Daerden *et al.*, "Pneumatic artificial muscles: Actuators for robotics and automation," *Eur. J. Mech. Environ. Eng.*, vol. 47, no. 1, pp. 11–21, 2002.